

High-resolution laser spectroscopy of diamagnetic helium in the chaotic regime

K. Karremans, W. Vassen, and W. Hogervorst

Department of Physics and Astronomy, Vrije Universiteit, De Boelelaan 1081, 1081 HV Amsterdam, the Netherlands

(Received 27 May 1999)

We measured a series of spectra of diamagnetic helium under fixed classical conditions. We varied the scaled energy from $\varepsilon = -0.40$ to -0.26 in steps of 0.02, which corresponds to a gradual increase of the number of chaotic orbits in classical phase space. The classical dynamics of the system is studied using closed-orbit theory. The high resolution of the experiment allows for an investigation of the evolution of the V_1^1 orbit and its repeated traversals. Taking only this stable orbit into account, we reconstruct the most pronounced peaks in the energy spectrum recorded at $\varepsilon = -0.36$. The accuracy of our experiment, confirmed by agreement with quantum helium calculations of action spectra up to scaled action 25, provides a good testing ground for recently developed uniform semiclassical approximations in closed-orbit theory. [S1050-2947(99)07412-0]

PACS number(s): 32.60.+i, 05.45.-a, 03.65.Sq, 32.80.Rm

I. INTRODUCTION

The diamagnetic Rydberg atom, a quantum-mechanical system with chaotic dynamics in the semiclassical limit, is a prototype system to investigate “quantum chaos” [1,2]. Classically, irregular motion arises when the spherical Coulomb term in the Hamiltonian becomes of the same order of magnitude as the cylindrical diamagnetic term, a situation which can easily be created in an experiment with Rydberg atoms. The scaling properties of Rydberg atoms can be used to perform experiments under fixed classical conditions. In such experiments the field strength γ ($\gamma = B/2.35 \times 10^5$ T) is adapted to the laser frequency exciting the Rydberg atom (excitation to energy E) in order to keep the scaled energy $\varepsilon = E\gamma^{-2/3}$ constant [3]. In the field-free case ($\varepsilon = -\infty$), classical phase space is completely regular. Above $\varepsilon = -0.5$, the fraction of classically chaotic trajectories gradually increases with scaled energy. According to closed-orbit theory, photoabsorption spectra near the ionization limit possess large-scale structures corresponding to the underlying classical dynamics [4,5]. In constant scaled-energy experiments, each classical electron orbit that starts at and returns to the nucleus contributes a sinusoidal oscillation to the absorption spectrum. In the Fourier transform of an absorption spectrum, the so-called action spectrum, peaks appear at the classical scaled actions \tilde{S} of closed electron orbits. This implies that the spectral resolution determines the maximum action that can be observed in an experiment. The amplitude of the recurrence peaks in such an action spectrum is related to the stability of the orbit, i.e., to the divergence of the adjacent electron trajectories.

In a hydrogen experiment by the Welge group in Bielefeld at constant scaled energy [6], spectra were recorded using a pulsed laser source and varying the scaled energy from -0.50 to $+0.02$ in steps of 0.05. This covers the region where most classical orbits are stable ($\varepsilon < -0.50$) up to completely chaotic phase space ($\varepsilon > -0.11$). The position of the recurrence peaks in the action spectra could be interpreted with closed-orbit theory up to $\tilde{S} = 5$. By increasing ε the creation and evolution of orbits could be followed in the experimental action spectra. In the $\varepsilon =$

-0.12 spectrum an exotic orbit turned up before its classical bifurcation energy of $\varepsilon = -0.115$. However, due to experimental uncertainties ($\delta\varepsilon = 0.005$) this peak could not be attributed unambiguously to a so-called ghost orbit. In the regular regime ghosts of rotator orbits were observed in several experiments, for the first time by van der Veldt *et al.* [7]. Comparison of recurrence amplitudes showed that closed-orbit theory predicts unphysical divergences at bifurcation energies. Uniform semiclassical approximations provide a correction of these amplitudes for orbits close to their bifurcation [8,9]. In addition to the correction for the unphysical divergences in the recurrence spectra the repaired closed-orbit formulas also give a description of ghost orbits.

The resolution of hydrogen experiments was not sufficient to investigate the long-time behavior of trajectories. In action spectra of high-resolution experiments on nonhydrogenic atoms, orbits could be followed up to considerable higher scaled actions than before. In helium experiments at $\varepsilon = -0.7$ [7], almost each peak could be attributed to a hydrogenic orbit, but around $\tilde{S} \sim 10$ additional peaks were observed at the sum of actions of two hydrogenic orbits [10]. These peaks result from core scattering, i.e., the electron scatters from one hydrogenic orbit into another. A quantum treatment of core scattering in closed-orbit theory shows the influence of the quantum defect on the recurrence amplitude [11–13]. This improved theory showed excellent agreement with singlet helium experiments in an electric field [14]. In another series of measurements the increasing differences with hydrogen were demonstrated in intensities of peaks in action spectra when larger quantum defects are involved [15].

In this paper we present results of high-resolution experiments in a magnetic field performed at higher scaled energies. In the regime of mixed regular and chaotic motion eight different spectra are recorded, varying the scaled energy from $\varepsilon = -0.40$ to -0.26 . R -matrix calculations are used to check the accuracy of the experiment. Due to the high resolution, recurrence peaks up to action 150 could be observed. As the limits of semiclassical theory are not well understood, the question arises up to what time scale classical trajectories can be extracted from a quantum spectrum. Especially cha-

otic orbits become of fundamental interest, because conceptual problems arise at time scales exceeding the Heisenberg time $t_H \sim \hbar/\Delta E$ (where ΔE is the typical level spacing). One of the challenges of the present work was to perform closed-orbit calculation up to high actions to obtain agreement with experiment not only in position but also in recurrence strength. The recently developed correction formula for the parallel orbit was applied to improve the agreement in electric-field experiments [16]. For diamagnetic Rydberg atoms in the chaotic regime also other types of uniform semiclassical approximation have to be applied to predict the recurrence strength connected to the perpendicular and exotic orbits.

This paper is organized as follows. In Sec. II we describe how closed-orbit theory reveals information on the classical dynamics from a photo-absorption spectrum. The setup for our diamagnetic experiment is presented in Sec. III. The experimental results are given in Sec. IV. We compare the action spectra with R -matrix calculations and use closed-orbit theory to interpret the data. Finally, we present some conclusions in Sec. V.

II. THEORY

A. Classical dynamics of diamagnetic hydrogen

Action spectra of Rydberg atoms in an external field reveal the underlying classical dynamics. Recurrence peaks can be attributed to classical closed orbits, trajectories starting at and returning to the nucleus. Application of semiclassical theory therefore begins with finding these orbits for the hydrogen problem. Differences between nonhydrogenic and hydrogenic action spectra are caused by core scattering. This possibility of scattering at the ionic core can be calculated via an iterative procedure [11–13]. For the small quantum defect $\delta = 0.068$ of the Rydberg series of the present experiment, this will give only minor differences compared to the hydrogenic action spectra, and this contribution will be neglected here.

The nonrelativistic Hamiltonian of a hydrogen atom in a magnetic field directed along the z axis for an $M_L=0$ transition is (in atomic units, $\gamma=B/2.35 \times 10^5$ T)

$$H = \frac{p^2}{2} - \frac{1}{r} + \frac{1}{8} \gamma^2 \rho^2. \quad (1)$$

When scale transformations $\tilde{r} = \gamma^{2/3} r$ and $\tilde{p} = \gamma^{-1/3} p$ are applied, a scaled Hamiltonian results:

$$\tilde{H} = \frac{\tilde{p}^2}{2} - \frac{1}{\tilde{r}} + \frac{\tilde{\rho}^2}{8}. \quad (2)$$

The classical dynamics of the scaled equations of motion do not depend on energy and field strength independently, but solely on the scaled energy $\varepsilon = E \gamma^{-2/3}$. Defining the classical scaled action of a closed orbit as

$$\tilde{S}(\varepsilon) = \frac{1}{2\pi} \oint \tilde{p} d\tilde{q} = \frac{S \gamma^{1/3}}{2\pi} \quad (3)$$

results in a parameter independent of the field strength.

Under fixed classical conditions, Planck's constant defines an absolute scale in the quantum Hamiltonian. As a consequence quantum conditions depend on the field strength, which can be quantified by defining the effective constant of Planck with

$$[\tilde{r}, \tilde{p}] = i \gamma^{1/3} = i \hbar_e. \quad (4)$$

The important trajectories in semiclassical calculations, the closed orbits, are searched for by numerical integration of the equations of motion up to a maximum scaled action. Varying the initial launching angle $\theta_i = \arctan(p_\rho/p_z)$ with steps of 0.0002° , the region between 0° and 90° is scanned for the scaled-energy range in the experiment. By numerically integrating the equations of motion problems arise at the Coulomb singularity, which can be avoided using a transformation to semiparabolic coordinates $u = \sqrt{\tilde{r} + \tilde{z}}$ and $v = \sqrt{\tilde{r} - \tilde{z}}$ and by applying a time transformation $dt = 2\tilde{r} d\tau$ [12]. The regularized Hamiltonian represents then a system of two coupled harmonic oscillators:

$$h = \frac{1}{2}(p_u^2 + p_v^2) - \varepsilon(u^2 + v^2) + \frac{1}{8}u^2v^2(u^2 + v^2) = 2. \quad (5)$$

The classical Hamilton equations of motion $dq_i/d\tau = \partial h/\partial p_i$ and $dp_i/d\tau = -\partial h/\partial q_i$ are given by

$$\begin{aligned} \frac{du}{d\tau} &= p_u, & \frac{dp_u}{d\tau} &= 2\varepsilon u - 4u v^2(2u^2 + v^2), \\ \frac{dv}{d\tau} &= p_v, & \frac{dp_v}{d\tau} &= 2\varepsilon v - 4v u^2(2v^2 + u^2). \end{aligned} \quad (6)$$

In Fig. 1 the scaled actions of the closed orbits found in the integration routine are plotted for different scaled-energy values. The step size of the sixth-order Runge-Kutta integration routine is chosen to have an accuracy up to the sixth digit in the classical scaled action. By evaluating the divergence of the adjacent trajectories, the stability of an orbit is determined. The scaled-energy variation from $\varepsilon = -0.40$ to -0.26 probes phase space, where the fraction of irregular orbits is increasing from roughly 40% to 80% [17]. For chaotic systems, long-period closed orbits are difficult to find because they become increasingly unstable. This was observed in a preliminary calculation with a larger step size for the launching angle, where some closed orbits were not found in the integration routine at actions above $\tilde{S}=6$. The evolution of closed orbits nicely follows from Fig. 1. At low scaled energies ($\varepsilon \rightarrow -\infty$) the only existing orbits are the one perpendicular (R^1) and the one parallel (V^1) to the magnetic-field axis. When the scaled energy is raised, new orbits are created from these two orbits. Vibrator orbits bifurcate out of the parallel orbit, whereas the perpendicular orbit generates rotator orbits. Holle *et al.* [3] classified these direct bifurcations from the parallel and perpendicular orbits. The rotator orbits, labeled R_k^n , are created in the k th bifurcation of the n th traversal of the perpendicular orbit (R^n). In the bifurcation diagram, e.g., the first bifurcation of the second traversal of the perpendicular orbit, R_1^2 , appears at $\varepsilon = -0.316$. The vibrator orbits are labeled likewise, i.e., V_k^n for the k th bifurcation from the n th return of the parallel orbit

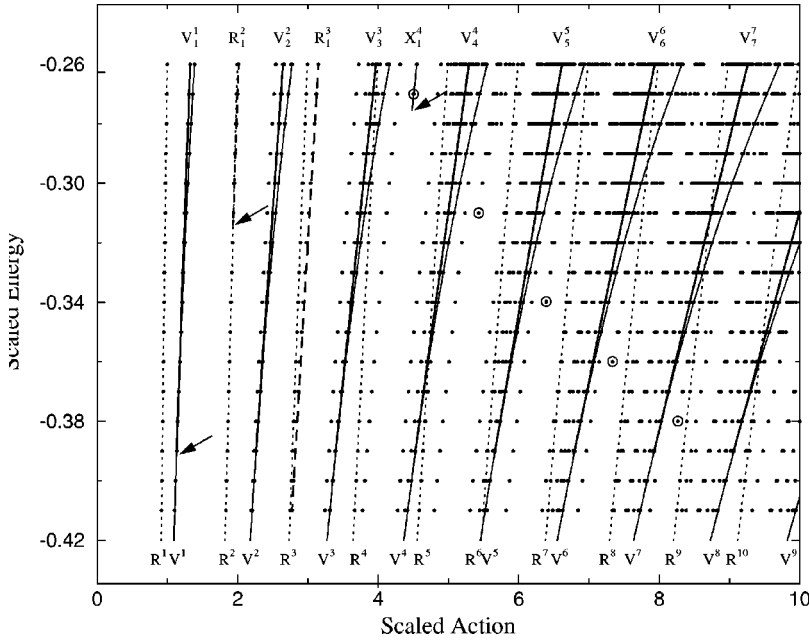


FIG. 1. Diagram of closed orbits up to scaled action $\tilde{S}=10$ in the scaled energy range of the experiment. Important orbits are labeled and represented by lines. The V_1^1 orbit and its repetitions (bold) bifurcate at $\varepsilon = -0.391$ from the parallel orbit, whereas the bifurcation of the R_1^2 orbit from the perpendicular orbit is visible at $\varepsilon = -0.314$. Exotic orbits (points marked with a circle) suddenly appear in this range several times, for instance at $\varepsilon = -0.276$ where the X_1^4 orbit bifurcates.

(V^n). The V_1^1 orbit and its higher-order returns ($n \times V_1^1 = V_n^n$), which turned out to be important in our experimental range, bifurcate from the parallel orbit at $\varepsilon = -0.392$. Rotator and vibrator orbits not only bifurcate from the perpendicular or parallel orbit but can also bifurcate from each other. For these orbits a labeling does not exist. Initially a new orbit starts at the same angle and consequently has the same action. When the scaled energy is increased the angle between the orbits gradually changes, resulting in an increasing difference in their scaled action.

Another class of orbits is formed by the exotics, which seem to appear out of nowhere in the bifurcation diagram. Holle *et al.* [3] labeled them in order of appearance with increasing action. This labeling becomes rather complicated when going to high actions. Therefore, we introduce the notation of an exotic to be X_k^n , where the subscript denotes the k th bifurcation (toward increasing ε) of an exotic in the region between two consecutive traversals of the perpendicular orbit (R^n and R^{n+1}), and the superscript n corresponds to the index of the perpendicular orbit (R^n). In the bifurcation diagram the exotic X_1^4 is visible at $\varepsilon = -0.27$ ($\varepsilon_{\text{bif}} = -0.276$) at a scaled action of $\tilde{S} = 4.51$. In the Fourier transform of a scaled-energy spectrum, peaks appear at the scaled action of classical closed orbits. The bifurcation scheme will be used to connect experimental recurrence peaks with classical electron orbits.

B. Closed-orbit theory

The relationship between classical trajectories and quantum spectra for Rydberg atoms in an external field is given by closed-orbit theory. This semiclassical theory was initially developed for constant fields by Du and Delos [4,5], and was subsequently transformed to describe scaled-energy experiments [6]. Experiments under fixed classical conditions have the advantage of resolving rapidly evolving orbits. Here we give a brief description of the theory, and present formulas valid for spectra at constant scaled energy.

According to closed-orbit theory, excitation of an atom produces an outgoing Coulomb wave. Sufficiently far away

from the core ($r > 50a_0$), the wave front, representing the motion of the electron, propagates along classical trajectories. Eventually some of the trajectories and their associated waves curve back to the nucleus, where they interfere with the outgoing Coulomb wave. The phase of the returning semiclassical wave of an orbit depends on S/\hbar , which is equal to $2\pi\tilde{S}/\hbar_e$. When recording a photo-absorption spectrum under fixed classical dynamics, the variation of \hbar_e generates oscillations of the form

$$f(\varepsilon, \hbar_e) = C_k^n(\varepsilon, \hbar_e) \sin \left[2\pi \frac{\tilde{S}_k^n(\varepsilon)}{\hbar_e} + \psi_k^n \right]. \quad (7)$$

The classical scaled action \tilde{S}_k^n of the n th return of the k th orbit determines the period of the sine oscillation on the $1/\hbar_e$ scale (or $\gamma^{-1/3}$ scale). The additional phase ψ_k^n is calculated from the Maslov index and other geometric considerations. The recurrence amplitude C_k^n contains information on the stability of the orbit via J_{12} , an element of the semiclassical Jacobian in (u, v) space, and the initial and final angles ($\theta_i^k, \theta_f^{k,n}$) of the orbit and the geometry of the transitions

$$C_k^n(\varepsilon, \hbar_e) = g_k 2^{19/4} \pi^{3/2} (\sin \theta_i^k \sin \theta_f^{k,n})^{1/2} \times \frac{Y(\theta_i^k) Y^*(\theta_f^{k,n})}{\sqrt{2^{1/2} J_{12}(k, n)}} \sqrt{\hbar_e}, \quad (8)$$

$$C_0^n(\varepsilon, \hbar_e) = g_0 2^{9/2} \pi \frac{Y(0) Y^*(0)}{|2^{1/2} J_{12}(0, n)|} \hbar_e.$$

Here the statistical weight g_k takes into account that for each orbit in the interval $0^\circ \leq \theta \leq 90^\circ$, an equivalent orbit in the interval $90^\circ \leq \theta \leq 180^\circ$ exists. Therefore, $g_k = 2$ for each orbit with $0^\circ \leq \theta < 90^\circ$, whereas $g_k = 1$ for the perpendicular orbit. The subscript $k=0$ indicates the parallel orbit. Note that this orbit has a different dependence on \hbar_e compared to the off-axis orbits, and that all oscillations vanish when the semiclassical limit is approached ($\hbar_e \rightarrow 0$). To remove the

magnetic-field dependence from the amplitude of orbits having $\theta \neq 0$ Main *et al.* [6] introduced a reduced absorption rate $R(\varepsilon, \hbar_e)$. This allows for a comparison of action spectra in different \hbar_e regimes:

$$R(\varepsilon, \hbar_e) = \frac{f(\varepsilon, \hbar_e)}{\sqrt{\hbar_e}} = \sum_{n,k} D_k^n(\varepsilon) \sin \left[2\pi \frac{\tilde{S}_k^n(\varepsilon)}{\hbar_e} - \frac{\pi}{2} \mu_k^n - \frac{3}{4} \pi \right] + \sum_n D_0^n(\varepsilon) \sqrt{\hbar_e} \sin \left[2\pi \frac{\tilde{S}_0^n(\varepsilon)}{\hbar_e} - \frac{\pi}{2} \mu_0^n - \frac{1}{2} \pi \right]. \quad (9)$$

Here the Maslov index μ_k^n is obtained by counting the number of times the orbit is crossed by its adjacent trajectories. The reduced recurrence amplitude $D(\varepsilon)$ is the amplitude $C(\varepsilon, \hbar_e)$ corrected for the \hbar_e dependence. Orbits with $\theta \neq 0$ contribute a constant sinusoidal oscillation to the reduced absorption spectrum, whereas the oscillation of the parallel orbit increases with $\sqrt{\hbar_e}$. For typical experimental scans ($\Delta \hbar_e^{-1} \approx 10$), the varying amplitude of the parallel orbit can be replaced by its average value.

The classical electron orbits follow from a scaled-energy absorption spectrum by Fourier transformation. The (squared) Fourier transformation of an experimental absorption spectrum in the \hbar_e^{-1} scale gives the action spectrum. The resolution in the absorption spectrum ($\delta \hbar_e^{-1}$) determines the maximum action at which recurrence peaks may be observed:

$$\tilde{S}_{\max} = \frac{1}{2\delta \hbar_e^{-1}}. \quad (10)$$

Therefore, a spectrum with a resolution $\delta \hbar_e^{-1}$ can be reconstructed by a summation over each orbit up to this maximum scaled action \tilde{S}_{\max} . In the calculation we stop the integration routine at \tilde{S}_{\max} ; so only a small fraction of the infinite sum of closed orbits is considered.

To calculate the amplitude for multiple traversals of an orbit, we stop the integration of the equations of motion at the first closure. The recurrence amplitude for repetitions of the orbit can be obtained from the stability matrix $J(k)$ of this trajectory. In these calculations a distinction is made between stable and unstable (chaotic) orbits. The stability of an orbit is deduced by inspecting the trace of the stability matrix $\text{Tr} J(k)$. Detailed formulas can be found in Refs. [6] and [18]. For unstable ($|\text{Tr} J(k)| > 2$) periodic orbits, it can be shown that

$$J_{12}(k, n) = \left| \frac{\sinh(\beta)}{\sinh(n\beta)} \right|^{1/2} J_{12}(k, 1), \quad (11)$$

with β a stability exponent. At $\varepsilon = -0.28$ the V_1^1 orbit, e.g., is unstable and the divergence of the adjacent trajectories results in an exponential decay in the recurrence amplitude with increasing n , as can be seen in Fig. 2(b).

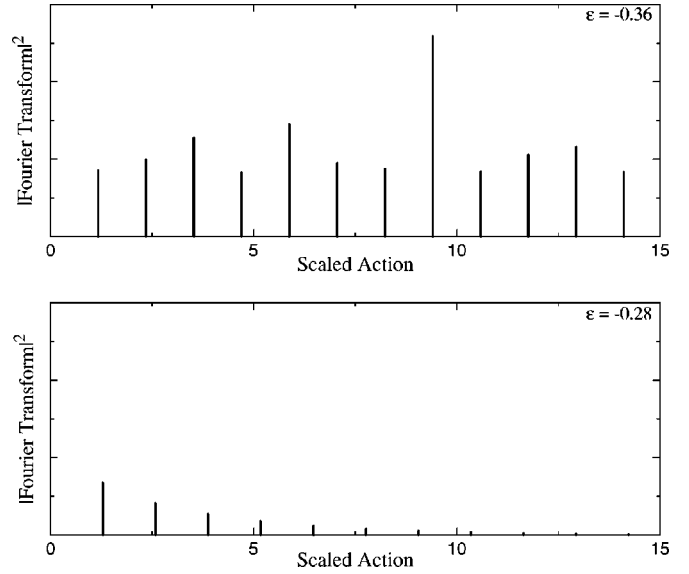


FIG. 2. Classical amplitude of the V_1^1 orbit for n repeated traversals at $\varepsilon = -0.36$ (stable) and $\varepsilon = -0.28$ (unstable).

The recurrence amplitude of repeated traversals of stable [$|\text{Tr} J(k)| < 2$] orbits behaves differently. In this case,

$$J_{12}(k, n) = \left| \frac{\sin(\alpha)}{\sin(n\alpha)} \right|^{1/2} J_{12}(k, 1), \quad (12)$$

where α is the winding number. As a result the recurrence amplitude as a function of the number of repetitions behaves quasiperiodically. This can be seen in Fig. 2, where we plotted the amplitude behavior of the V_1^1 orbit when still stable ($\varepsilon = -0.36$). With increasing ε the winding number varies continuously. Then for each value of n there exists a scaled energy value for which

$$n\alpha = m\pi, \quad m = 1, 2, \dots, n > 1. \quad (13)$$

At these ε values the recurrence amplitude of the n th return will then explode. Evaluation of the adjacent trajectories of this orbit shows that together they form a focus exactly at the nucleus at the n th return. At such a focus point, the approximation of returning wave by a pencil of classical electron trajectories produces unphysical results. Such divergences are familiar in geometrical optics, where infinite intensity occurs when a plane wave is focused to a point. Gao and Delos used the connection with diffraction theory to construct uniform approximations [19].

Another manifestation of a failure of closed-orbit theory is the observation of ghost orbits. In the Fourier transform of experimental and quantum R -matrix spectra, peaks can be attributed to orbits at energies where they are classically forbidden. A continuation of closed-orbit theory to complex phase space demonstrates that the contribution of complex orbits becomes important close to a bifurcation [8,20]. Complex ghosts of rotator and vibrator orbits are in general hidden by real closed orbits with nearly the same scaled action. Exotic orbits, on the other hand, appear out of nowhere and their isolated positions in the bifurcation diagram make them particularly suitable for studying the behavior of ghosts.

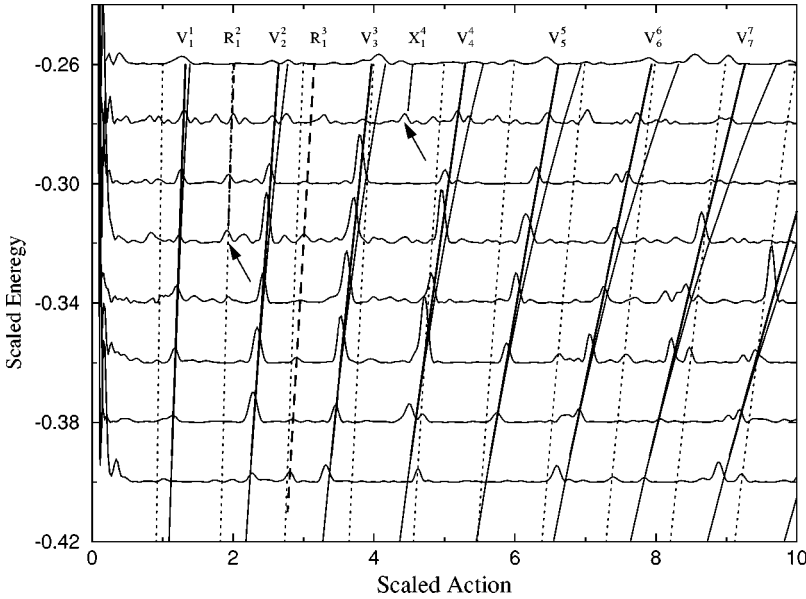


FIG. 3. The experimental action spectra in the scaled-energy range $-0.40 \leq \varepsilon \leq -0.26$. The most pronounced peaks can be attributed to the V_n^n orbits. The quasiperiodic appearance in the range $-0.38 \leq \varepsilon \leq -0.30$ of this orbit reflects its stability. At $\varepsilon = -0.28$ (arrow) a recurrence peak is already visible before the bifurcation energy of the exotic X_1^4 orbit. A peak at $\varepsilon = -0.32$ (arrow) corresponds to the ghost of a rotator orbit.

III. EXPERIMENTAL SETUP

Our experimental setup was described in detail in a previous paper on scaled-energy experiments in the regular regime [21]. Here we only give a brief summary.

In a crossed laser-atomic-beam experiment, $M_L = 0$ Rydberg atoms are excited ($\lambda = 260$ nm) from the metastable 2^3S_1 state (triplet helium) in the presence of a magnetic field. The metastable state is populated in a dc discharge running through an expanding gas flow. The transition to the 2^3P_2 state is used for transverse laser cooling of the triplet helium atoms. For this purpose a single-mode diode laser (SDL-6702-H1) generates 30-mW output power at 1083 nm. This laser is locked to the $2^3S_1 \rightarrow 2^3P_2$ transition using saturated absorption spectroscopy in a helium rf discharge. The diverging beam is collimated in two dimensions applying the curved-wave-front technique over a cooling length of 18 cm [22]. The highly parallel beam results in a reduction of the Doppler-broadened linewidth at 260 nm, whereas the increase of atomic density gives rise to a signal increase of a factor 10. The decrease in laser-cooling performance due to the nearby electromagnet is removed by mounting a mu-metal shielding. A pinhole placed at 30 cm from the gas nozzle prevents the atomic beam from damaging the excitation box. This stainless-steel box (at +30 V) is carbon coated to reduce the stray-electric field ($F < 5$ mV) in the excitation region. An UV laser beam, produced by intracavity frequency doubling a cw ring dye laser (3 mW, 260 nm) perpendicularly intersects the beam of metastable atoms. The excited Rydberg atoms move 12 cm into a low-magnetic-field region before they are ionized by an electric field between the excitation box and a quadrupole mass filter. The He^+ ions pass this mass-selective filter before they are counted with an electron multiplier.

In the scaled-energy experiments the field strength is adjusted at each frequency step of the laser. The relative laser frequency is determined by counting the fringes of a 150-MHz etalon. At the start of a laser scan the recording of a zero-magnetic-field Rydberg level provides an absolute frequency reference. The relative variation of the scaled energy during a 30-GHz laser scan is $\delta\varepsilon = 0.0001$, whereas the ab-

solute accuracy of the scaled energy during the total scan is estimated to be $\delta\varepsilon = 0.0002$. The constant-scaled-energy scans start at principle quantum number n corresponding to a magnetic field of 0.31 T ($\hbar_e^{-1} = 91$). This implies that for higher scaled energies experiments start at higher n values [$n = 1/(\hbar_e \sqrt{-2\varepsilon})$]. Therefore, the experimental resolution of low scaled-energy spectra is better, and consequently the maximum scaled action reached will be somewhat higher.

IV. RESULTS

A. General view

We measured absorption spectra at constant scaled energy for eight different values of ε . The magnetic-field strength was varied during the experiments from 0.31 to 0.21 T (corresponding to \hbar_e^{-1} ranging from 91 to 103). The regime of mixed regular and chaotic classical motion is explored varying the scaled energy from $\varepsilon = -0.40$ to -0.26 with steps of 0.02. Multiplying the experimental spectra with a sine window before they are Fourier transformed reduces the effect of spectral leakage [21]. The intensity of each experimental spectrum is normalized to the corresponding quantum R -matrix calculation for helium. The good general agreement, up to scaled action 15, between experimental action spectra and spectra obtained by R -matrix quantum calculation, demonstrates the accuracy of our experiment. The squared Fourier transforms of the experimental spectra up to scaled action 10 are reproduced in Fig. 3. The noise level, determined by fluctuations in laser power and atomic beam density, is considered to be constant over the whole ε range. The width of the recurrence peaks ($\Delta\tilde{S} = 0.1$) is determined by the length of the spectrum in \hbar_e^{-1} .

The bifurcation diagram in Fig. 1 is used to assign closed orbits to the recurrence peaks. The most prominent recurrence peaks are connected to the V_1^1 orbit and its repeated traversals (V_n^n). This orbit bifurcates out of the parallel orbit at $\varepsilon = -0.391$. Above this energy the parallel orbits (V_n^n) become unstable, but the exponential decrease in the recurrence strength of the repeated traversals is masked by the

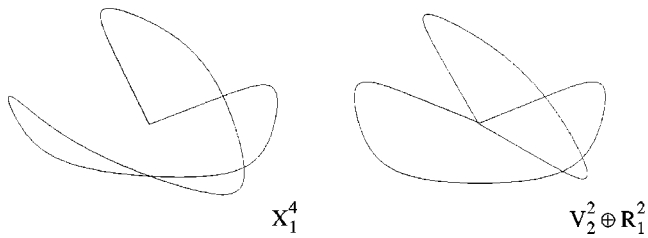


FIG. 4. The trajectory of the exotic X_1^4 orbit at $\varepsilon = -0.27$ is presented in semiparabolic coordinates (u, v) . The sum orbit of the periodic R_1^2 and V_1^2 orbits has the same scaled action $\tilde{S} = 4.51$ as this exotic orbit. The shape of this combination of orbits shows a remarkable similarity to the exotic orbit.

more intense V_n^n orbits. The action spectra in the regime from $\varepsilon = -0.38$ to -0.30 show the evolution of the V_1^1 orbit and its higher harmonics. When the scaled energy is increased the recurrence peaks connected to the V_n^n orbit appear at higher scaled actions. The quasiperiodicity of these recurrence peaks reflects the stability of this trajectory, which becomes unstable at $\varepsilon = -0.289$. Above this scaled energy the recurrence amplitudes of repeated traversals of this orbit decrease exponentially, and V_1^1 and its recurrences no longer contribute significantly to the action spectra.

In the $\varepsilon = -0.32$ action spectrum a recurrence peak appears at $\tilde{S} = 1.92$. Although its position coincides with the repeated traversal of the perpendicular orbit, we cannot assign this peak to the R^2 orbit. When an atom is excited from an s state to a p state, the perpendicular orbit lies exactly in the node of the outgoing wave function, resulting in zero recurrence strength in closed-orbit calculations. However, the weak recurrence strength found in quantum R -matrix calculations shows that approximating the returning wave by the central orbit only is not correct. Modifications to closed-orbit theory can be implemented, which provide good agreement with quantum calculations [23]. Although these weak recurrences have never been resolved in any experiment, the combined effect of the perpendicular orbit together with a ghost of a rotator orbit has been observed [7,24,21]. The scaled energy $\varepsilon = -0.32$ is close to the bifurcation energy

$\varepsilon_{\text{bif}} = -0.317$ of the R_1^2 orbit, sometimes referred to as a ‘‘Pac-Man’’ orbit because of its shape in ρ and z coordinates.

Therefore, we attribute the recurrence peak at $\tilde{S} = 1.92$ to the combination of the second traversal of the perpendicular orbit and the ghost of this Pac-Man orbit. To our knowledge, closed-orbit calculations have never successfully incorporated both effects simultaneously. For this reason we searched for isolated recurrences, connected to ghosts of exotic orbits. The recurrence peak at scaled action $\tilde{S} = 4.51$ of the exotic X_1^4 orbit is already visible at $\varepsilon = -0.280$ below its classical bifurcation energy ($\varepsilon_{\text{bif}} = -0.276$). Before we attribute the appearance of this peak to the precursor (ghost) of an exotic orbit, we must point out that for nonhydrogenic atoms this exotic is not observed isolated from other recurrences. Due to the possibility of core scattering, the combination of the V_1^2 orbit ($\tilde{S} = 2.51$) and the R_1^2 orbit ($\tilde{S} = 2.00$) has a sum action $\tilde{S} = 4.51$, exactly equal to the scaled action of the exotic orbit.

Figure 4 shows that the shape of the X_1^4 orbit is surprisingly similar to the trajectory followed in the sum orbit $V_1^2 \oplus R_1^2$. The recurrence at $\tilde{S} = 4.51$ is therefore connected to a combination of two processes: core scattering responsible for the sum orbit, and a tunnelinglike phenomenon giving rise to the ghost of the exotic.

B. Comparison with R -matrix quantum calculations

Various methods have been developed to calculate the energy levels of diamagnetic Rydberg atoms. For levels below the ionization limit, the diagonalization of the Hamiltonian in a Sturmian basis is the simplest technique. The R -matrix formalism is used to calculate the eigenstates of nonhydrogenic atoms. We used the computer code of Ref. [25] to calculate scaled-energy helium spectra in the experimental regime $\hbar_e^{-1} = 91\text{--}103$. The square of the Fourier transform of such spectra provides the quantum helium action spectra presented in Fig. 5.

The recurrence peaks in the quantum action spectra show a general good agreement in position and strength with our

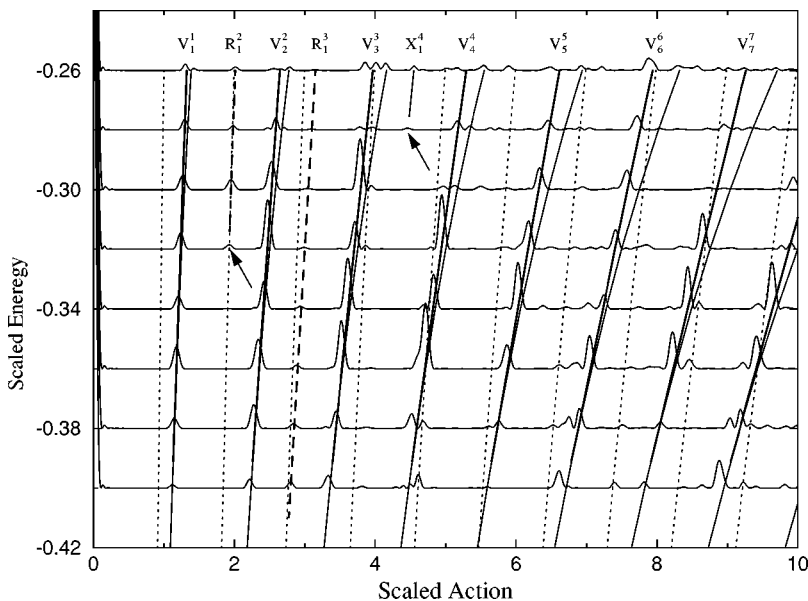


FIG. 5. Action spectra obtained from helium R -matrix calculations in the scaled-energy regime $-0.40 \leq \varepsilon \leq -0.26$ show a good resemblance with the experimental results (Fig. 3). Recurrences marked with an arrow are connected to ghost orbits.

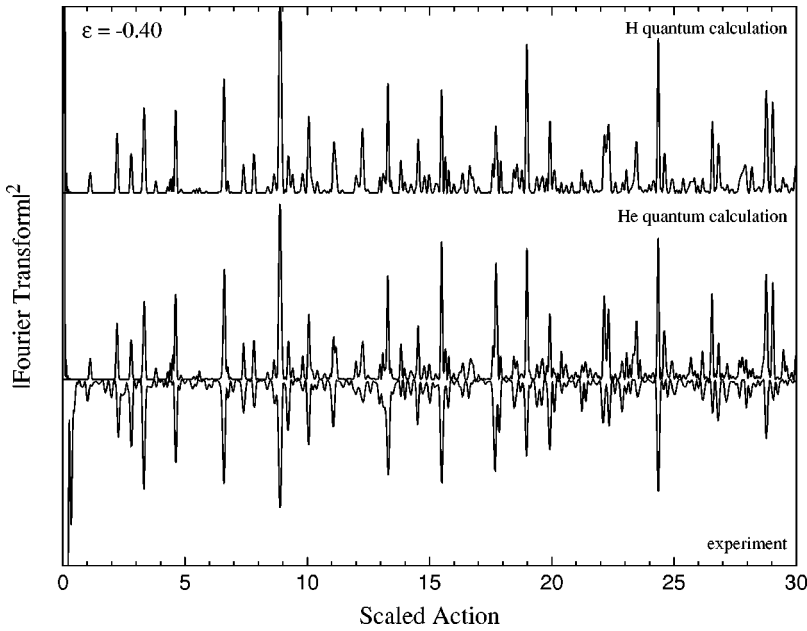


FIG. 6. Comparison of the experimental action spectrum at $\varepsilon = -0.40$ up to high scaled action with spectra from R -matrix calculations for H and He. Differences in recurrence strength between hydrogen and helium calculations are caused by core-scattering.

experiment. In the absence of experimental noise, small peaks such as, e.g., the very weak recurrences of the perpendicular orbit (R''), are observable, although not visible on the scale of this overview. Furthermore ghost peaks at scaled energies even further away from the bifurcation are revealed. The precursor of the exotic orbit X_1^4 at $\tilde{S} = 4.51$, observed in the experiment at $\varepsilon = -0.28$, is already visible in the quantum spectra at $\varepsilon = -0.30$, whereas the ghost of the R_1^2 Pac-Man orbit can already be seen in the $\varepsilon = -0.34$ action spectrum.

The high resolution in the experiment ($\delta\hbar_e^{-1} \approx 0.003$) allows us to observe recurrence peaks up to much higher actions than in the earlier hydrogen experiments. At $\varepsilon = -0.40$, the experimental resolution of $\delta\hbar_e^{-1} \approx 0.003$ gives, according to Eq. (10), rise to a maximum scaled action of $\tilde{S}_{\max} \approx 150$. We performed numerical calculations at $\varepsilon = -0.40$ for hydrogen and helium in the experimental range. The calculated action spectra are presented in Fig. 6.

Up to action 25 no significant differences are found comparing the R -matrix calculations of helium with hydrogen. This result shows that the process of core scattering can be neglected even at high actions for this scaled energy. Therefore, hydrogenic closed-orbit calculations should be sufficient to construct action spectra of helium. When the quantum helium action spectra are compared with the experimental results, good agreement exists up to $\tilde{S} = 25$. Differences between quantum helium calculations and experiment caused by experimental variations in ε , become increasingly important toward higher actions. This comparison underlines the high accuracy for the experimental value of ε which can be used to test closed-orbit theory up to high actions.

Since the action spectra of hydrogen show very good agreement with our helium experiments we can compare our data with the results of hydrogen experiments at the same scaled energy performed by Holle *et al.* [6]. We chose a scaled energy of $\varepsilon = -0.3$ as hydrogen data are published for this value. The experimental helium action spectrum at $\varepsilon = -0.3$ is in good agreement with the Fourier transform of

helium R -matrix calculations performed in the experimental \hbar_e^{-1} regime (91–103), as shown in the upper part of Fig. 7.

The hydrogen experiments were performed at different magnetic field strengths, 2.7 and 6 T [6], with a resolution that revealed recurrences up to scaled action 5. The Fourier transform of the quantum hydrogen calculation at $\varepsilon = -0.30$ in this experimental \hbar_e^{-1} range (33–43) reproduces the experimental action spectrum ($\tilde{S} < 5$) for hydrogen at this scaled energy very well. Furthermore, the calculated spectrum also allows comparison at higher actions. To investigate the influence of the different quantum conditions, we also calculated the hydrogen spectrum for \hbar_e^{-1} ranging from 91 to 103. Both hydrogenic action spectra are given in the lower part of Fig. 7. The action spectra are normalized to the peak connected with the V_1^1 orbit (at $\tilde{S} = 1.26$) to remove the \hbar_e scaling of the off-axis orbits. These reduced action spectra allow for a direct comparison between calculated hydrogen and helium data.

Peaks in the action spectrum of hydrogen and helium occur at the same position, but pronounced differences are found in the intensities. The high resemblance in position of the recurrence peaks for different atomic species, even at different magnetic-field strengths, demonstrates the invariance of the underlying classical dynamics. The high similarity in the hydrogenic and helium action spectra in the same \hbar_e range shows the small influence of the ionic core. However, differences between hydrogen and helium in the $\varepsilon = -0.30$ case become prominent at actions significantly lower than in the $\varepsilon = -0.40$ case. Already at scaled action $\tilde{S} = 3.8$, intensity differences between hydrogen and helium appear. The position of this recurrence is exactly at the sum of actions of recurrence peaks at $\tilde{S} = 1.3$ and 2.5. The process of core scattering gives rise to a sum orbit with an action equal to the sum of two hydrogenic orbits. The oscillation produced by this orbit interferes with the hydrogenic contribution, resulting in a decreased intensity. At higher scaled energies the number of orbits increases, giving a larger effect of combinations of orbits.

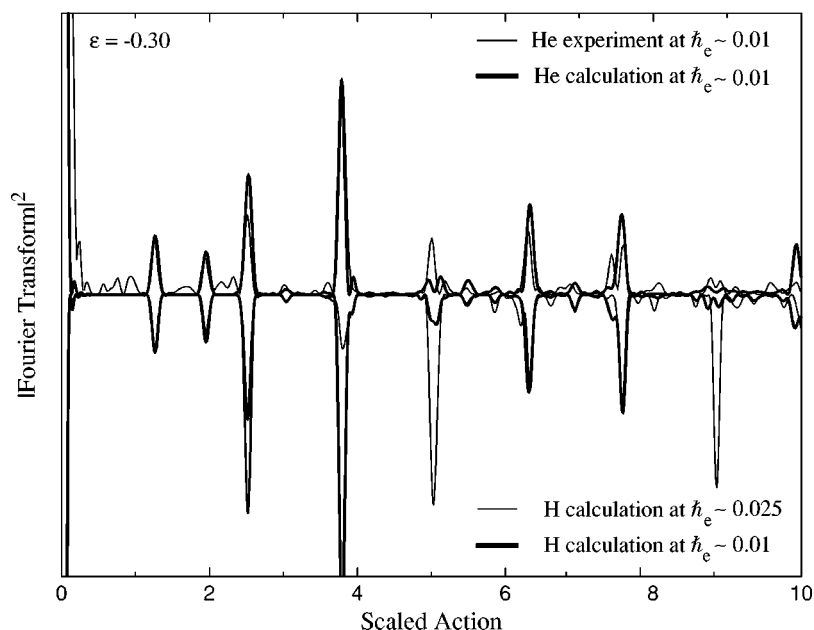


FIG. 7. Action spectra of hydrogen and helium at $\varepsilon = -0.30$. Under constant quantum conditions (same \hbar_e) the helium spectra show a high resemblance to hydrogen. The differences between the hydrogenic action spectra at $\hbar_e \sim 0.025$ and 0.01 are due to interferences of orbits.

In the following we neglect the process of core scattering and concentrate on the more prominent differences between hydrogen action spectra in the different \hbar_e regimes. Significant differences arise at scaled actions $\bar{S} = 2.5, 3.8, 5.0,$ and 8.8 . Semiclassical calculations show that at these actions several classical orbits contribute to a single recurrence peak (see Fig. 1). The recurrence strength of a combination peak is the square of the coherent summation of recurrence amplitudes connected to the unresolved orbits. According to Eq. (9), the phase of oscillation connected with an orbit depends on \hbar_e . This formula furthermore shows, that in the semiclassical limit $\hbar_e \rightarrow 0$ small action differences between unresolved orbits give rise to enhanced phase differences. As a consequence the interference of orbits generates different results for different quantum conditions. In the simplest situation of two interfering orbits the oscillation of the recurrence strength as a function of \hbar_e^{-1} has been observed experimentally [21]. The differences between our helium results and

previous hydrogen experiments are mainly due to the different quantum conditions, and not to core effects.

C. Comparison with closed-orbit theory

We applied closed-orbit theory to reconstruct the action spectra of helium at $\varepsilon = -0.40$. In an R -matrix calculation for $\varepsilon = -0.40$, only minor differences are found between the experimental action spectrum and hydrogen quantum calculations. The R -matrix calculations form a good representation of the experimental action spectrum up to action 10. Therefore, we restrict ourselves to closed-orbit theory for hydrogen and neglect the process of core scattering. The results of standard closed-orbit theory are presented in Fig. 8(a). The position of the calculated peaks is in good agreement with R -matrix calculations for hydrogen in Fig. 8(c) and our experiment in Fig. 8(d). Large discrepancies are found for several recurrence strengths.

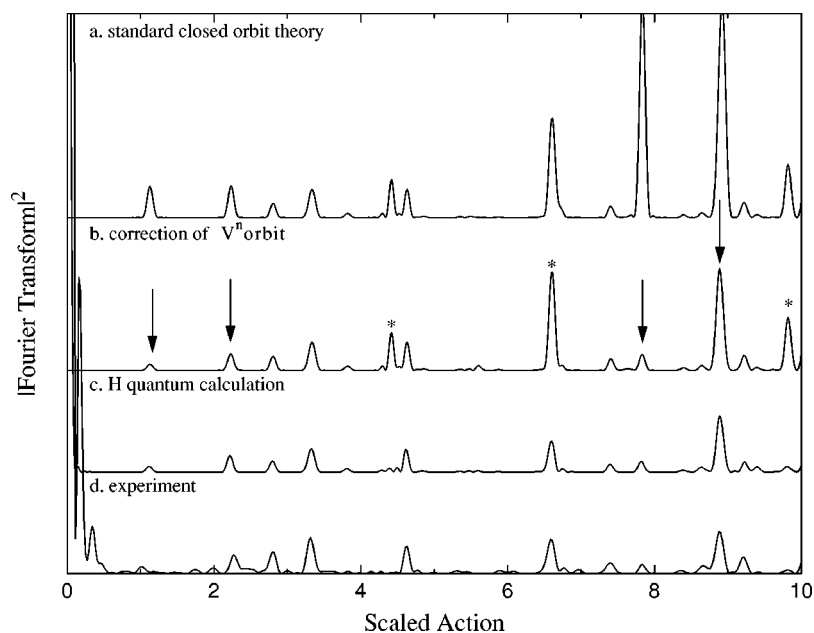


FIG. 8. Comparison of closed-orbit calculations at $\varepsilon = -0.40$ with R -matrix calculations for hydrogen. Uniform approximations for the parallel orbit reduce the recurrence strength of the diverging peaks (arrows). To increase the agreement, additional repair of diverging off-axis orbits (asterisks) is required.

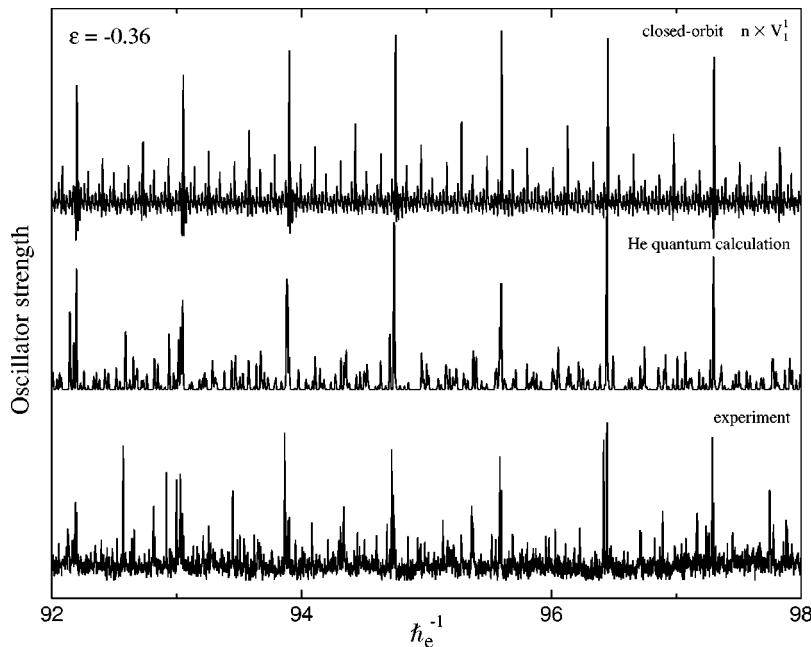


FIG. 9. Comparison of oscillator strength spectra at $\varepsilon = -0.36$. The prominent equidistant peaks in the experimental spectrum are reproduced by quantum helium calculation. This harmonic-oscillator-like structure is reproduced in closed-orbit theory taking only the V_n^n orbits into account.

The intense peak in the closed-orbit calculations at $\tilde{S} = 7.83$ is connected with the seventh traversal of the parallel orbit (V^7). Here adjacent trajectories form a focus which gives rise to a divergence in the semiclassical amplitude. Repair of this cusp catastrophe by applying the uniform semiclassical approximation [9] results in an intensity reduction of this peak by more than a factor 10. The action spectrum in Fig. 8(b) shows that the repair of the parallel orbits gives rise also to intensity correction for the V^1 , V^2 , and V^8 recurrence peaks (at $\tilde{S} = 1.12$, 2.24, and 8.89, respectively). The uniform approximation for the parallel orbits results in a better agreement between semiclassical theory and quantum R -matrix calculations. However, closed-orbit calculations fail to predict the recurrence strength of peaks marked with an asterisk. At higher action $\tilde{S} > 10$ an increasing number of diverging peaks arises from closed-orbit calculations. All these peaks correspond to off-axis orbits close to a bifurcation. For instance the peak at $\tilde{S} = 4.42$ results from the orbit which starts under an angle of 28.8° . These bifurcations from off-axis orbits likewise result in diverging amplitudes for the recurrence peaks. Uniform approximations for off-axis orbits are required, but the technique is not yet available.

D. Construction of narrow absorption lines with closed-orbit theory

Instead of constructing action spectra, closed-orbit theory can also be used the other way round to reconstruct low-resolution spectra with the same set of trajectories. In high-resolution experiments, the maximum scaled action becomes large, and it is not feasible to search for all closed orbits. In our experiment the stable V_1^1 orbit and its repeated traversals are prominently present in the action spectra, so we can indicate structures in the energy spectra which can directly be attributed to this orbit.

The experimental spectrum at $\varepsilon = -0.36$, shown in Fig. 9, clearly shows a harmonic-oscillator-like structure. The separation between the most prominent peaks of 0.851 (in units

of \hbar_e^{-1}) matches precisely with the inverse action ($\tilde{S} = 1.175$) of the V_1^1 orbit. We constructed a spectrum considering only this orbit and its repeated traversals. The contribution of the stable V_1^1 orbit is, according to Eq. (9), a simple sine function with period $1/\tilde{S}$. The repeated traversals generate higher harmonics with periods $1/(n\tilde{S})$, with an amplitude given by Eq. (12). Including up to the 90th return of this orbit, the width of the theoretical peak matches our experimental resolution. A summation of these 90 sine functions gives rise to the upper spectrum in Fig. 9. The large peaks appear at the same \hbar_e^{-1} value as in the experimental spectrum. We also performed R -matrix calculations for hydrogen and helium at $\varepsilon = -0.36$. Both quantum calculations showed the same harmonic-oscillator-like structure as in our experiment. The theoretical helium spectrum convoluted with a Gaussian window of 10 MHz is also shown in Fig. 9. So the position of the most important peaks in the experiment and in quantum calculations can be easily reproduced in a closed-orbit spectrum considering only a single electron orbit. In the regime of mixed regular and chaotic motion, the contribution of this stable orbit can be identified straightforwardly in the spectra. This particular spectrum at $\varepsilon = -0.36$ demonstrates that the energy levels of the system are dominated by orbits in only a tiny fraction of phase space.

V. CONCLUSIONS

We have performed constant scaled-energy spectroscopy on diamagnetic helium in the range from $\varepsilon = -0.40$ to -0.26 . The experimental spectra were interpreted using closed-orbit theory for hydrogen. Due to the high spectral resolution of our experiment, recurrence peaks even above scaled action 100 are resolved. Comparison of the experimental action spectra with R -matrix calculations for hydrogen and helium underlines the accuracy of our measurements. At $\varepsilon = -0.40$ the experiment is in good agreement with both quantum calculations up to scaled action $\tilde{S} = 25$, indicating that core effects are negligible. Applying closed-

orbit theory at $\varepsilon = -0.40$ gives good agreement with the positions of peaks in the action spectrum. Uniform semiclassical approximations for the parallel orbit significantly improve the agreement in recurrence strength. However, the failure to predict recurrence strengths of off-axis orbits close to a bifurcation shows that other correction mechanisms are required.

For increasing scaled energies, core effects become prominent at lower action. At $\varepsilon = -0.28$ the observation of the ghost of an exotic is obscured by the occurrence of sum orbits at the same scaled action ($\tilde{S}=4.5$). However, in an R -matrix analysis of previous hydrogen and present helium experiments at $\varepsilon = -0.30$, the most prominent differences could be attributed to differences in the \hbar_e value. In the overview of the experimental action spectra, the evolution of the V_n^n orbit can be clearly recognized. The quasiperiodic structure of this orbit and its repeated traversals in the range $-0.38 \leq \varepsilon \leq -0.30$ shows that this orbit is stable. For higher

scaled energies this is no longer the case, indicating that the V_1^1 orbits has become chaotic. The harmonic-oscillator structure in the photo-absorption spectrum at $\varepsilon = -0.36$ is directly related to this V_n^n orbit. The prominent absorption lines are easily reconstructed with closed-orbit theory, taking only the V_n^n orbit into account.

ACKNOWLEDGMENTS

The authors wish to thank Jacques Bouma for his excellent technical support, and acknowledge Aschwin Wijnsma for his assistance in the construction of the laser-cooling section. We would like to thank John Shaw for making available his closed-orbit calculations, and Dominique Delande for providing the source code for the R -matrix calculations. Financial support from the Foundation for Fundamental Research on Matter (FOM) is gratefully acknowledged.

-
- [1] M. C. Gutzwiller, *Chaos in Classical and Quantum Mechanics* (Springer-Verlag, New York, 1990).
 - [2] H. Friedrich and D. Wintgen, *Phys. Rep.* **183**, 37 (1989).
 - [3] A. Holle, J. Main, G. Wiebusch, H. Rottke, and K.H. Welge, *Phys. Rev. Lett.* **61**, 161 (1988).
 - [4] M.L. Du and J.B. Delos, *Phys. Rev. A* **38**, 1896 (1988).
 - [5] M.L. Du and J.B. Delos, *IEEE J. Quantum Electron.* **24**, 1455 (1988).
 - [6] J. Main, G. Wiebusch, K. Welge, J. Shaw, and J.B. Delos, *Phys. Rev. A* **49**, 847 (1994).
 - [7] T. van der Veldt, W. Vassen, and W. Hogervorst, *Europhys. Lett.* **21**, 9 (1993).
 - [8] J. Main and G. Wunner, *Phys. Rev. A* **55**, 1743 (1997).
 - [9] J.A. Shaw and F. Robicheaux, *Phys. Rev. A* **58**, 1910 (1998).
 - [10] D. Delande, K.T. Taylor, M. Halley, T. van der Veldt, W. Vassen, and W. Hogervorst, *J. Phys. B* **27**, 2771 (1994).
 - [11] P.A. Dando, T.S. Monteiro, D. Delande, and K.T. Taylor, *Phys. Rev. Lett.* **74**, 1099 (1995).
 - [12] P.A. Dando, T.S. Monteiro, D. Delande, and K.T. Taylor, *Phys. Rev. A* **54**, 127 (1996).
 - [13] P.A. Dando, T.S. Monteiro, and S.M. Owen, *Phys. Rev. Lett.* **80**, 2797 (1998).
 - [14] A. Kips, P.A. Dando, W. Vassen, and W. Hogervorst, *Phys. Rev. A* **58**, 3043 (1998).
 - [15] M. Keeler and T.J. Morgan, *Phys. Rev. Lett.* **80**, 5726 (1998).
 - [16] A. Kips, W. Vassen, and W. Hogervorst, *Phys. Rev. A* **59**, 2948 (1999).
 - [17] W. Schweizer, R. Niemeier, G. Wunner, and H. Runner, *Z. Phys. D* **25**, 95 (1993).
 - [18] T. van der Veldt, Ph.D. thesis, Vrije Universiteit Amsterdam, 1993.
 - [19] J. Gao and J.B. Delos, *Phys. Rev. A* **56**, 356 (1997).
 - [20] M. Kuś, F. Haake, and D. Delande, *Phys. Rev. Lett.* **71**, 2167 (1993).
 - [21] K. Karremans, W. Vassen, and W. Hogervorst, *Phys. Rev. A* **60**, 2275 (1999).
 - [22] W. Rooijackers, W. Hogervorst, and W. Vassen, *Opt. Commun.* **123**, 321 (1996).
 - [23] J.A. Shaw, J. Delos, M. Courtney, and D. Kleppner, *Phys. Rev. A* **52**, 3695 (1995).
 - [24] H. Held, J. Schlichter, G. Raithel, and H. Walther, *Europhys. Lett.* **43**, 392 (1998).
 - [25] M. Halley, D. Delande, and K.T. Taylor, *J. Phys. B* **26**, 1775 (1993).